Biomass Conversion and Biorefinery
https://doi.org/10.1007/s13399-023-04057-4

ORIGINAL ARTICLE

Conversion of corn shell as biomass solid waste into carbon species for efficient decontamination of wastewater via heavy metals adsorption

Ayman F. Abou-Hadid[1] · Usama A. El-Behairy[1] · Mahmoud M. Elmalih[2] · Enas Amdeha[3] · Ahmed M. A. El Naggar[3] · Mohamed H. Taha[2] · Ahmed E. M. Hussein[2]

Received: 18 October 2022 / Revised: 27 February 2023 / Accepted: 10 March 2023
© The Author(s) 2023

Abstract
Biomass-based solid residuals can be of serious hazardous environmental impacts if left for natural degradation. Thus, the proper utilization of such residuals is highly recommended. Therefore, one of solid residuals: namely, corn shell, was used in this study to synthesize carbon species (labeled as CS-C) as an adsorbent for efficient removal of heavy metal ions from aqueous solution. The structural properties and the textural characteristics of the prepared carbon species were verified. The present charges on the carbon surface were acquired via zeta potential analysis. The performance of CS-C, as adsorbent, was investigated through batch technique. Adsorption isotherm was optimally described using the Langmuir model reflecting that the removal process occurs at the homogenous surface of CS-C through a chemical reaction (surface complexation mechanism). The equilibrium state for the sorption process was reached after 4 h of interaction. The kinetic studies revealed the nice fit of heavy metal removal process to Pseudo-second-order model and the thermodynamics is matched to endothermic, spontaneous, and feasible sorption process. The displayed results could emphasize the high potentiality of CS-C to act as a remarkable sorbent for efficient tackling of water contaminants.

Keywords Adsorption · Biomass · Carbon species · Decontamination · Heavy metals · Wastewater

1 Introduction

The United Nations considered water security as one of the 17 sustainable development goals (SDGs: 6). Wastewater treatment is an important aspect of water security. Aquatic environment contamination with heavy metals is a global problem [1, 2]. Radioactive nuclides and hazard elements, for instance cadmium and radioactive species, are characterized by non-biodegradable, high persistence, and bioaccumulation; therefore, they dramatically affect the aquatic food chain [2–4]. Industrial pollution such as pigment works, electroplating, and metallurgical alloying, as well as the nuclear activities such as radioactive mining, nuclear power plant, and radioactive waste disposal are the main source for water contamination [3–7]. Wastewater treatment becomes a vital issue for developing countries in regards to the water as well as environmental securities. Conventional techniques such as solid–liquid extraction [8, 9], liquid–liquid extraction [10, 11], precipitation [12, 13], and sorption [14, 15] have been applied for heavy metals removal from aqueous solution. Although these technologies are frequently used, they have intrinsic disadvantages, e.g., high-energy requirements, byproduct formation, and high sludge production [3–8].

The adsorption of heavy metals from aqueous solutions was established as a superior technique to other methods and has received recent interest since it is a simple, effective, inexpensive, recyclable, and environmentally friendly procedure [16–18]. The adsorption effectiveness of several adsorbents for removing heavy metals from an aqueous solution has been examined [17–20]. It is general knowledge that

✉ Enas Amdeha
enas_amdeha@yahoo.com

✉ Ahmed M. A. El Naggar
drmeto1979@yahoo.com

[1] Faculty of Agriculture, Ain Shams University, Cairo, Egypt

[2] Nuclear Materials Authority, El Maddi, P.O. Box 530, Cairo, Egypt

[3] Egyptian Petroleum Research Institute (EPRI), 1 Ahmed El-Zomor St, Nasr City, Cairo, Egypt

Published online: 20 March 2023

the adsorbent selection is critical to the adsorption behavior. Typical adsorbents like activated carbon and zeolite cannot keep up with the demand since they produce a lot of sludge during the removal process, limiting their adsorption impact [12–14]. As a result, developing a variety of unique, ecofriendly adsorbents to provide efficient heavy metals removal is of major importance.

Biomass materials as the substrate of adsorbent composites have garnered a lot of interest in the field of environmental management, among other useful materials [21, 22]. Because of their accessible availability and excellent adsorption capabilities, biomass-based carbon compounds, which may be generated from agricultural and forest products, have sparked widespread concern [21–23]. The recycle of natural waste to meet the goal of environmental conservation has been the subject of extensive investigation. Biochar made from forestry wastes has been found to provide potential marketing advantages for the adsorption process due to its low cost, eco-friendly, and natural availability [23].

Because of their plentiful pore structure, large specific surface area, and other properties, carbon species are considered as an effective adsorbent. As a result, many carbon species have been reported to be used in wastewater treatment [24, 25]. Furthermore, carbon obtained from biomass resources provides a novel method for maximizing the value of biomass waste. From the standpoint of recycling resources, the use of organic waste to make biochar has recently piqued interest. It is feasible to employ organic waste as a biochar precursor [26, 27]. As a result, the use of these materials in the remediation of environmental pollution has recently gotten a lot of attention. Treatment of these wastes properly results in high-value-added products.

One of the food crops with the greatest global distribution is corn. The typical method for getting rid of corn residues involves burning them off in the air, which frequently pollutes the environment. The capacitive performance of corn shells—the outer layer of corn ears—was studied. Corn shells contain a lot of carbon and can be turned into porous carbon [28]. They are mainly constituted by lignocellulose and has hydroxyl and amino groups on their surface. However, the adsorb-ability is low and lacks selectivity when it is used as an adsorbent directly [29]. These reasons make the production of carbon species from agricultural waste an alternate form of disposal that indirectly lessens environmental issues [30].

Inspired by the aforementioned aspects, this work investigates the adsorption behavior of agricultural waste-based carbon material with a focus on its uptake of heavy metals such as Cd (II) and radioactive (VI) species from aqueous solution. Wherein, an agricultural waste (Corn Shell; CS) was used for the preparation of carbonaceous material by a simple thermal technique. TEM, BET, FTIR, XRD, DLS, and zeta analysis were performed to figure out essential characteristics of the prepared material. The novelty of this study is based on first reveal of corn shell (biomass solid residual) as a raw source for preparing carbon using moderate temperature at which construction of carbon geometry and rearrangement of its particles had taken place. Also, the presented carbon species, as adsorbent, have versatile functional groups which enhance their efficiency towards heavy metals removal.

2 Experimental

2.1 Materials

All chemicals were of the reagent grade and were used directly. The used chemicals were hydrochloric acid (HCl, (≥96%)), sodium hydroxide (NaOH, (≥98.5%)), $CdSO_4$, and $UO_2(NO_3)_2.6H_2O$ obtained from Fluka Chemika (Switzerland), which were utilized to prepare the heavy metals standard solutions of 1.0 g L^{-1}. All solutions were prepared using deionized (DI) water. Multi-component solution samples of cadmium and hazardous species ions synthesized via the stock solutions.

2.2 Preparation of waste-based carbon

In this study, carbon species produced from waste is offered as environmentally friendly adsorbent for removing radioactive species and cadmium species from aqueous solutions. In which, a valuable material natural carbon is made as a valuable material for uptake usages using corn shell (CS) as agricultural waste that was gathered from a farm in Al-Sharqia Governate, Egypt. The fresh waste was dried in an oven at 90 °C for 1 week. The dried sample was undergone calcination process for 6 h at 500 °C in a muffle furnace using 25 °C/min heating rate. The produced carbon (designated as CS-C) was obtained in a black color after cooling at room temperature [31].

2.3 Characterization

The prepared carbon was characterized by using various analytical tools. Diffractometer patterns of X-ray diffraction (XRD) were recorded (Shimadzu XD-1, Japan). Using a Nicolet Is-10 model infrared spectrophotometer (USA), KBr method was used to perform Fourier transform infrared (FTIR) spectroscopy. Using a NOVA 3200 apparatus (USA), nitrogen adsorption desorption isotherms at − 196 °C were used to determine the surface characteristics of the produced structures. Using transmission electron microscope (high-resolution), model JEM 1230, the study's reported structures' morphological properties were examined (JEOL, Japan). Using a dynamic light scattering (DLS) device, the zeta potential was determined (Malvern-ZS, Ltd., UK,

nano series). With the aid of a dispersive Raman spectrometer (BRUKER-SENTERRA, Germany) with an integrated microscope (Olympos), the phase of carbon was determined.

2.4 Sorption methodology

The sorption characteristics of CS-C towards heavy metals ions were performed in batch experiments at room temperature (25 ± 1 °C) using thermo shaker water bath (scientific precision SWB 27–27 L) in polypropylene tubes. The impact of solution pH (1–9) on the sorption process was carried out by adjusting the solution with 0.5 M HCl and 0.5 M NaOH. The equilibrium studies were performed using different metal ion concentrations (20–300 mg L^{-1}). Sorption kinetics was conducted at various reaction times (2–600 min). Briefly, definite weight of the sorbent (m, g) was shaken with definite volume of the multi-component solution (V, L) which contains initial concentration of Co (50 mg L^{-1}). All experiments were carried out at 12 h to confirm achieving the equilibrium. All tests were conducted three times, and only relative error mean value of ≤ 4% was accepted. The sorbent was removed from the aqueous solution by filtration, and ICP-AES (Optima 2100DV, Perkin-Elmer, USA) was used for measuring the residual concentration of heavy metals ions in the aqueous solution (Ce, mg L^{-1}). The sorption efficiency %, sorption capacity qe (mg g^{-1}), and the dimensionless distribution constant (K_C) were calculated from the following equations [32].

$$R\% = \frac{(C_o - C_e)}{C_o} \times 100 \tag{1}$$

$$q_e = (C_o - C_e) \times \frac{V}{m} \tag{2}$$

$$K_C = \left(\frac{q_e}{C_e} \times 1000\right) \tag{3}$$

2.5 Modeling of sorption process

2.5.1 Sorption isotherm models

The equilibrium experiments provide important data for plant design and improvement operational control. Accordingly, 0.1 g of CS-C was contact with 25 mL of multi-component solution contain various metal ion concentration (20–300 mg L^{-1}) of each metal ions at pH of 4.01 for 12 h at temperature of 25 ± 1 °C. Langmuir, Freundlich, and Temkin isotherm models were applied for describing the isotherm of cadmium and radioactive ions uptake process by CS-C. Table 1S displayed the applied non-linear equations of the isotherm models Table S1 [33–35].

Table 1 Characteristics of carbon produced from corn shell

S_{BET}, (m^2/g)	Total pore volume, (cm^3/g)	Average pore diameter, (nm)
11.30	0.034	12.32

2.5.2 Sorption kinetic models

The sorption kinetics is essential for better understanding the sorption mechanism and to figure out the reaction rate controlling step. In this regard, a set of experiments were performed by shaking 25 mL of the multi-component solution (50 mg/L initial concentration) and 0.1 g of CS-C at solution pH 4.01 and temperature 25 ± 1 °C for different interval times (2–600 min). Largergren, pseudo-second-order, and intraparticle diffusion (Weber and Morris) kinetic equations were used for analyzing the adsorption results. Table 1S displayed the applied non-linear equations of the kinetic models [33–35].

2.5.3 Appropriate the applied models

Chi-square (x^2) (Eq. 4) and coordination coefficient (R^2) (Eq. 5) were used for fitting the isotherm and kinetic models whereas the lowest (x^2) and the highest (R^2) values, meaning the good fitting to the experimental results [33, 34].

$$x^2 = \sum \left[\frac{\left(q_{exp} - q_{pred}\right)^2}{q_{pred}} \right] \tag{4}$$

$$R^2 = 1 - \frac{\sum_1^n \left(q_{exp} - q_{pred}\right)^2}{\sum_1^n \left(q_{exp} - \overline{q_{exp}}\right)^2} \tag{5}$$

where x^2 is Chi-square coefficient, the number of test points is n, the experimental equilibrium capacity is q_{exp} (mg g^{-1}), while the predicted capacity is q_{pred} (mg g^{-1}).

2.5.4 Sorption thermodynamics

The dependence of CS-C towards metal ions on the reaction temperature was investigated to explore the sorption thermodynamic performance. Accordingly, 25 mL of the multi-component solution (50 mg/L initial concentration) was contacted with 0.1 g of CS-C at pH of 4.01 for 240 min at different reaction temperatures 25⁻50 ± 1 °C. The thermodynamic parameters, namely, Gibbs free energy change ($\Delta G°$), standard enthalpy change ($\Delta H°$), and standard entropy change ($\Delta S°$) were evaluated using equations listed in Table 1S [35, 36].

3 Results and discussions

3.1 Sorbent characterizations

3.1.1 XRD

The structure of the prepared carbon can be analyzed through the XRD pattern, Fig. 1. The spectrum showed a broad peak in the range 18–38° due to the amorphous carbon structure for the lignin-based carbon. Also, it reflects the stacking of the graphitic plates [37]. The peaks occur near 2θ = 26.6° and 28.3° correspond to the (0 0 2) plane of the graphite and can be attributed to the graphitic region in the prepared carbon. The interlayer spacing d_{002} value is 0.32 nm. The peaks at ~ 41° and 50.2° correspond to the (1 0 0) planes, and the detected peaks at around 58.6° and 66° are assigned to the (0 0 4) planes; these peaks are for the graphitic structure and have also been observed in previous carbon experiments [38]. The peak at ~ 74° corresponds to the (1 1 0) plane in the carbon [39].

3.1.2 FTIR

The raw corn and the prepared carbon are tested using FTIR to ensure that all chemical groups besides carbon have been completely removed (Fig. 2). From Fig. 2a, it is found that the peaks at 3270 cm^{-1} and 2888 cm^{-1} are corresponded to the O–H H-bond of cellulose and C–H stretching vibration of cellulose and lignin, respectively. While, the absorption band at 1733 cm^{-1} is related to the C = O bond of hemicellulose-lignin linkages. The absence of these important peaks in the produced carbon (Fig. 2b) confirming the conversion of raw corn into carbon species. Moreover, a wideband with a sound intensity can be found at 3600–3850 cm^{-1} [39]. This band peak is due to the O–H vibrational stretching and bending mode of both the OH and H_2O that present due to moisture. Furthermore, this band has also been referred to the presence of the H–bonds between the OH groups [40]. The bands at 2900–3000 cm^{-1} and 1680 cm^{-1} are for C–H aliphatic axial deformation in CH_2 and CH_3 groups and C–O stretching vibration, respectively, in lignin, cellulose, and hemicelluloses [41, 42]. The peak at 1649 cm^{-1} is investigative to the amides that exist on the surface of the agro-waste-based carbon. The occurrence of this group might be happened through the thermal conversion process due to the existence of the primary amines that last in the agricultural-waste source [40]. The peaks at 1466 cm^{-1} and 1425 cm^{-1} can be attributed to the C–H bending vibration of CH_2 and the carboxyl groups, respectively [39]. The carbon fingerprint has a peak at about 1115 cm^{-1}. This band may also be connected to the stretching vibration of the C–O–C ring in both symmetric and asymmetric forms [38]. Besides, the peak at 1053 cm^{-1} is observed in the FTIR spectrum of lignin-based carbon indicating the presence of C–O groups and unconjugated C = O stretch [41]. In addition, other vibrations present underneath 900 cm^{-1} may be due to the C–H vibration.

3.1.3 Raman spectroscopy

Raman spectroscopy has been utilized to examine the prepared carbon structure because it is an appropriate method for assessing the structure and quality of carbon materials, as shown in Fig. 3. Two bands in the spectrum, the D band and the G band, which are associated to out-of-plane and in-plane sp^2 carbon bonds, respectively, show the basic characteristics of carbon materials [43]. The carbon hybridization (sp^2) and stretching mode in the C–C bond in graphitic materials are what cause the G band (1595 cm^{-1})

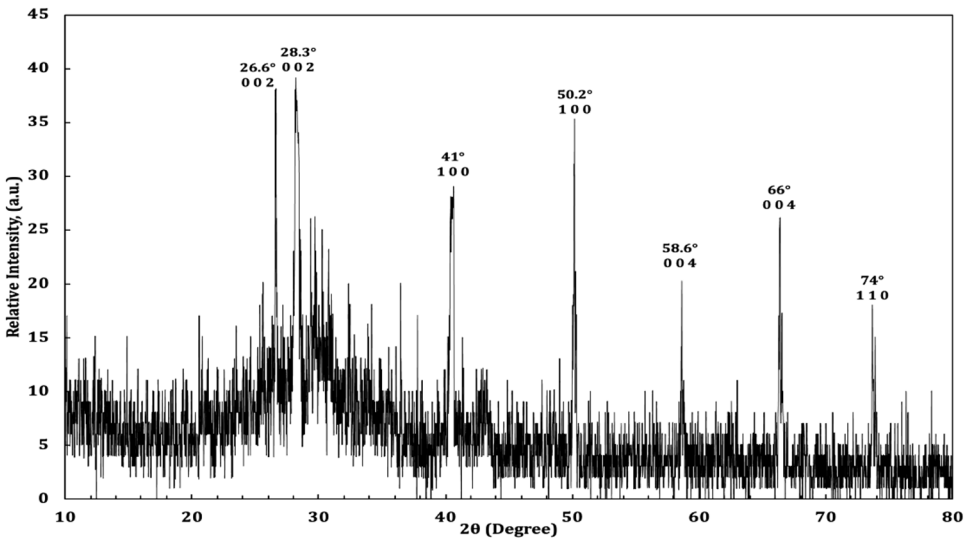

Fig. 1 XRD spectrum of carbon produced from corn shell

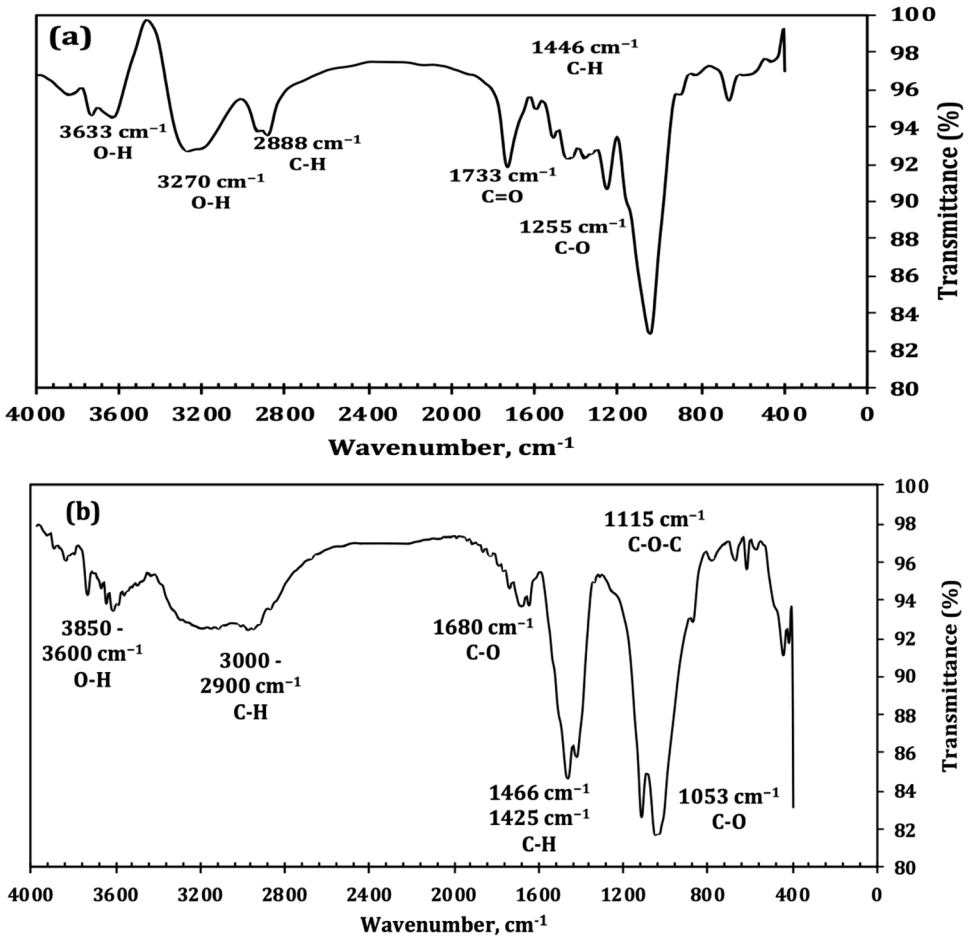

Fig. 2 FTIR spectrum of (**a**) corn shell. (**b**) Carbon produced from corn shell

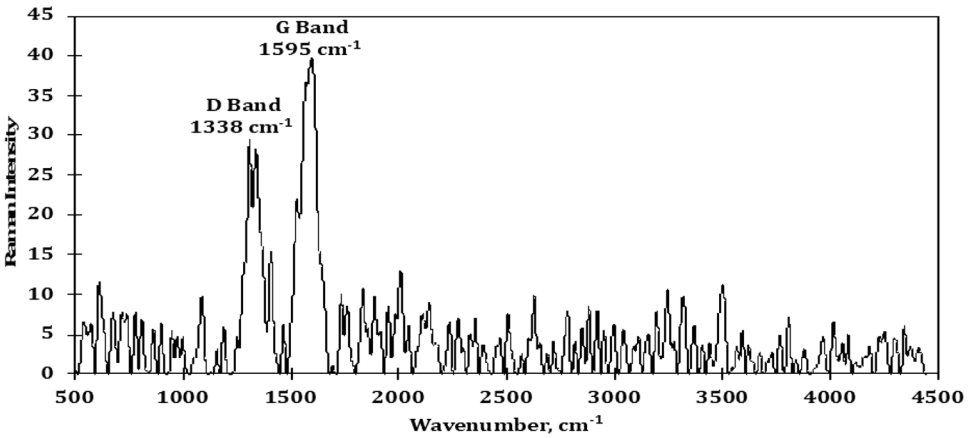

Fig. 3 Raman spectrum of carbon produced from corn shell

to exist, which explains the degree of graphitization [30, 38, 43]. While the D band (1338 cm^{-1}) is attributed to the E_{2g} phonon of $C_{sp}{}^2$ atoms and describes structural flaws and partially disordered structures [37]. The defects in the graphitized structure can be attributed to this band, which is also known as the "turbostratic carbon structure" [38]. The k-selection rule fails, resulting in the Raman intensity of the D band being inversely related to crystallite size. Any carbon sample's surface layer's crystallite size in this band's intensity can be estimated [41]. It is common practice to gauge the degree of structural disorder using the I_D/I_G ratio of peak intensities. This ratio is the ratio of the integrated Raman-allowed band intensity to the disorder-induced band intensity [44]. The relationship between the two band intensities is frequently used in literature as a gauge of structural order since it provides the count of structural flaws

and quantifies the measure of edge plane exposure [38]. A higher ratio of I_D/I_G corresponds to the carbon with more defects [42]. The I_D/I_G of the prepared carbon is equal to 0.78. Impurities such ions or oxygen superficial groups are blamed for some of the lesser peaks [40].

3.1.3.1 BET The isotherm and the surface area of the prepared carbon were studied by the N2 adsorption–desorption isotherm at – 196 °C, Fig. 4; Table 1. The Brunauer, Emmett, and Teller (BET) equation is applied [37]. Depending on the composition and carbonization conditions, the lignin-based adsorbent carbonized revealed various isotherms for porous materials such as types I, II, or IV [45]. In this study, the prepared carbon exhibits the type IV isotherm in the IUPAC classification, suggesting the existence of mesoporous on the carbon structure, and type H3 hysteresis that occurs when aggregates (loose assemblages) of plate-like particles forming slit-like pores.

The type H3 loop has two specific characteristics: The lower limit of the desorption branch is typically found at the cavitation-induced P/P_0, and the adsorption branch resembles a type II isotherm. Loops of this type can also occur if the pore network comprises of macropores that are not filled with pore condensate or non-rigid aggregates of plate-like particles, such as certain clays. The desorption branch's abrupt step-down is the H3 loop's defining characteristic [39]. The presence of pores inside the prepared carbon is a significant structural element that affects carbon characteristics. As shown from the pore size distribution figure, Fig. 4(b), the prepared carbon has mesopores with an average pore diameter of about 12.3 nm; this porosity of the lignin-based carbon boosted through the carbonization process by the elimination of volatile material [38].

3.1.4 Zeta potential

When a particle moves under the influence of an electrical field, the layer that stays attached to it has an electrical potential known as the zeta potential. When the suspension is steady and the absolute value of the zeta potential is more than 30 mV, the particles are evenly disseminated [44]. The study of the carbon's surface charge, which favors a positively charged metal's adsorption on heavy metals (positive surface charge), reveals that pHs in the range of (5–7) showed a strong negative zeta potential. Generally speaking, pH may be one element that, depending on the situation, can affect the adsorption process (Fig. 5).

3.1.4.1 TEM The microstructural characteristics of the prepared carbon are influenced by the precursor bio-charac-

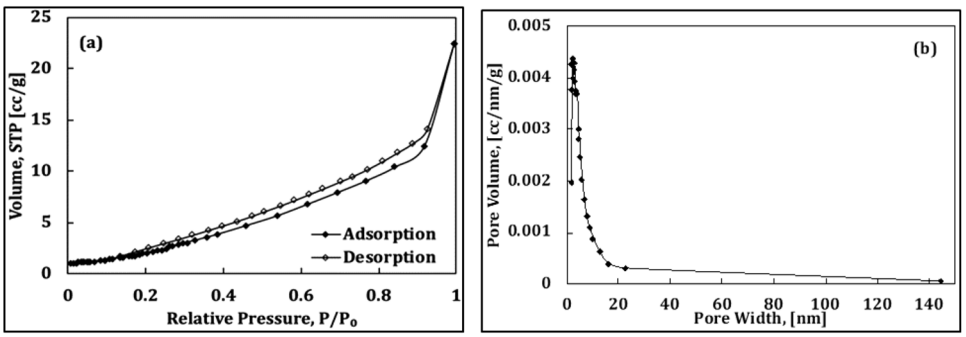

Fig. 4 (**a**) N2 adsorption–desorption isotherm at – 196 °C. (**b**) The pore size distribution curve of carbon from corn shell

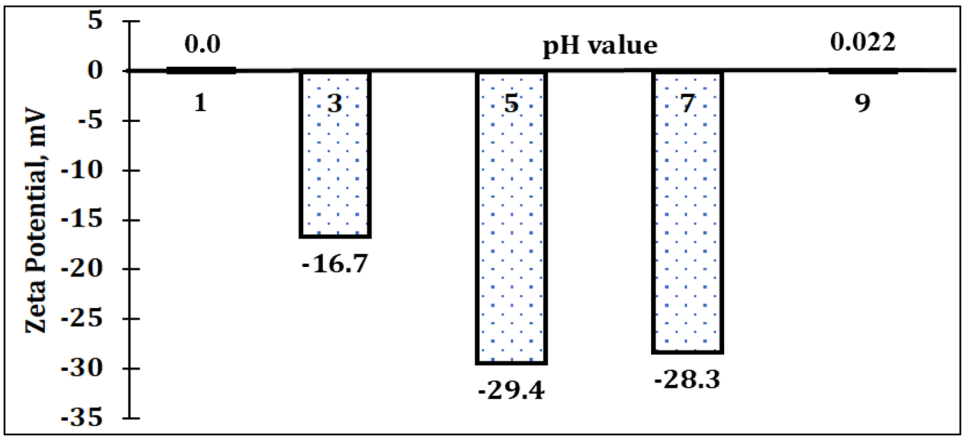

Fig. 5 Zeta potential of the carbon produced from corn shell as a function of pH

teristics wastes as well as the nature of the carbon before activation. The natural hierarchical structure of corn shell makes it a suitable carbon precursor to create porous carbon with improved adsorption performance. Corn shell is a bio-waste precursor for making carbon species and is made up of cellulose (43%), hemicellulose (31%), lignin (22%), and ash (1.9%) [40, 45]. Figure 6(a and b) show that corn shell-carbon consists of sphere-like nanoparticles (Nps) with diameters about 12 nm, which is coincident with the data from BET analysis. The TEM micrographs of carbon are shown to provide significant information concerning its surface morphology. The micrographs of the prepared carbon showed a relatively amorphous nature that could be observed; nevertheless, there are agglomerated particles forming clusters. In particular, Fig. 6(c, d) shows that the particles of the prepared carbon have a mixed nature of amorphous and crystalline appearance. Moreover, it shows how small crystals of various forms are found embedded among the big char particles.

3.2 Adsorption investigation

3.2.1 Effect of PH

Figure 7 obviously shows the sorption performance of CS-C as a function of solution pH. The test conditions were kept at shaking time of 12 h, initial concentration of 50 mg L^{-1}, sorbent dose of 4.0 g L^{-1}, and 25 ± 1 °C temperature, while solution pH was varied in the range of 1–9. The exhibited data explore that corn sorbent has the same sorption behavior towards both metal ions at solution pH in the range of 1–4, whereas the sorption efficiency increases to ~ 70% for cadmium(II) and ~ 92% for radioactive substances. However, the uptake performance is changed as the pH increase from 4 to 9 whereas (VI) sorption efficiency dramatically decreases to ~ 36% while the sorption efficiency of Cd(II) slightly increased to ~ 81% till solution pH of 7 then negatively impacted as the pH increases to 9. Since that the aqueous chemistry of the adsorbate and the chemistry of the sorbent surface, it is important to study the speciation of metal ions (50 mg L^{-1}) at HNO_3 (0.1 M) as a function of pH using

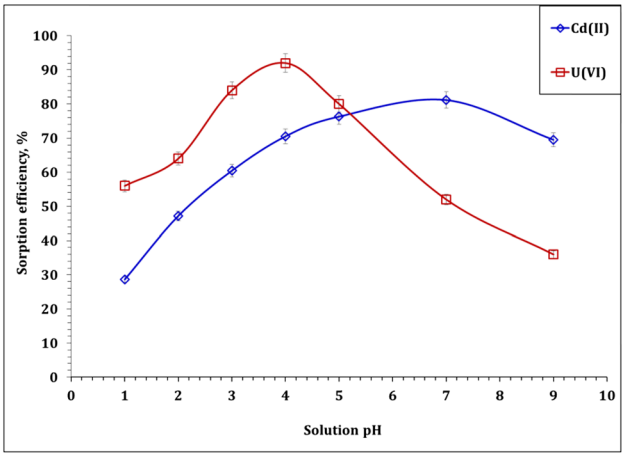

Fig. 7 Metal ions uptake percent dependence on solution pH (4.0 g sorbent/L; initial concentration 50 mg $L.^{-1}$; 12 h; temperature 25 ± 1 °C)

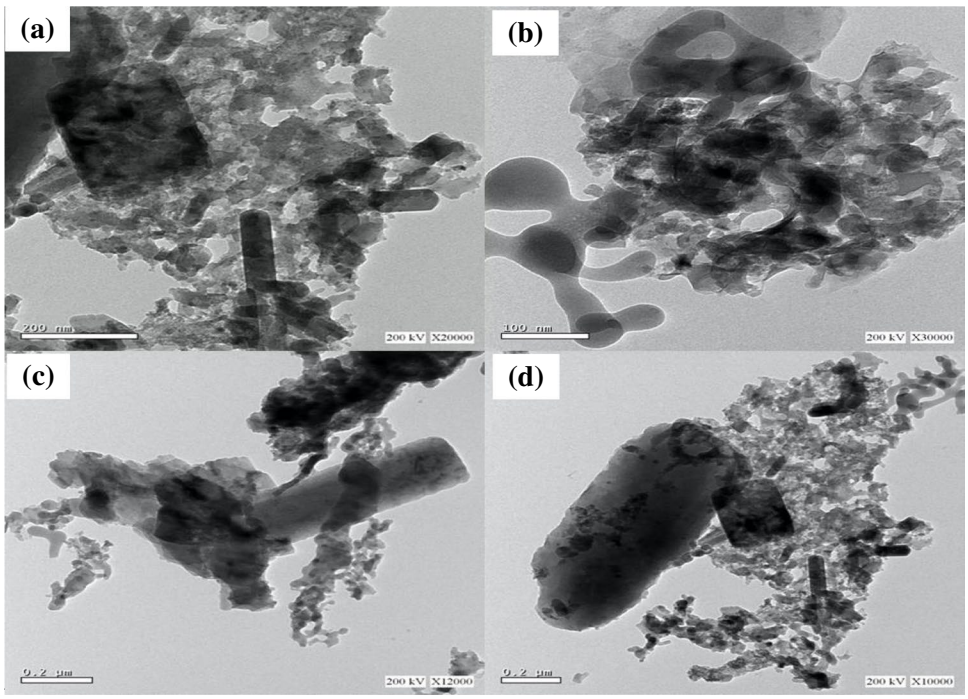

Fig. 6 TEM of the prepared carbon from corn shell

Medusa/hydra software Fig. (1S-I-II) [13]. The speciation of both metal ions declares that both metal ions show cationic species (mainly UO_2^{2+} and Cd^{2+}) at pH 1–4. Cadmium cationic species still the main species for further solution pH increase up to 8 then the insoluble species becomes the predominate species for pH higher than 8. The insoluble radioactive (VI) species becomes the main species as the solution pH increase over 4, while radioactive (VI) anionic species becomes predominate at pH higher than 10.

The sorption performance of corn carbon could be clarified in accordance to the zeta potential of the sorbent (Fig. 5) and the adsorbate species as a function of pH (Figs. 1S I–II). Specifically, the increase of pH value could be joined by obvious increase in the zeta potential value; however, the adsorbent conserved its negative charge. The increase of zeta potential value is referring to the high dispersion of the adsorbent into the media, thus increased activity could be noticed at higher pH values. On the other hand, the presence of negative charge on the adsorbent (at all pH values) is reflecting the sorbent high tendency towards the capture of positive cations. Additionally, the zero charge point of the adsorbent was found to be at pH value of 1 (Fig. 5). Therefore, noticeable decrease in the removal of positive cations could be generally observed at low pH values. The decrease of activity can be also explained by the high competition between hydrogen ions and the metals cations at the very strong acidic media (pH value around 1).

As the solution pH increases, the positive charge (hydrogen ions) decreases which freed many active surface sites and in turn enhances the sorption efficiency. Further increase in pH negatively impacts the sorption efficiency, whereas the cationic species disappears, and the insoluble radioactive (VI) species ($UO_2(OH)_2.H_2O$: at pH > 4) and cadmium(II) ($Cd(OH)_2$: at pH > 8) become the predominate (Fig. 2S-I). This performance was supported by previous study using biochars derived from corn straw silage [46], magnetic corn straw biochar composites [3], and oyster shell biochars [47] for cadmium removal from aqueous solutions, whereas Cd(II) sorption was pH-dependent. In addition, Aslani and Amik [17], Alahabadi et al. [48], and Li et al. [49] reported the same performance for (VI) radioactive species at various solution pH.

3.2.2 Adsorption isotherm

The sorption isotherm of metal ions using CS-C is represented by the illustration of the relation between sorption capacity (qe) against metal ion residual concentration (Ce) (Fig. 8). The experimental conditions were shaking time of 12 h, sorbent dose of 4.0 g L^{-1}, solution pH 4.01, 25 ± 1 °C temperature, and initial concentration range of 20–300 mg L^{-1}. The obvious data show that the sorption performance of both metals consists of two parts: The first part shows rapid increase of the sorption capacity which could be attributed to

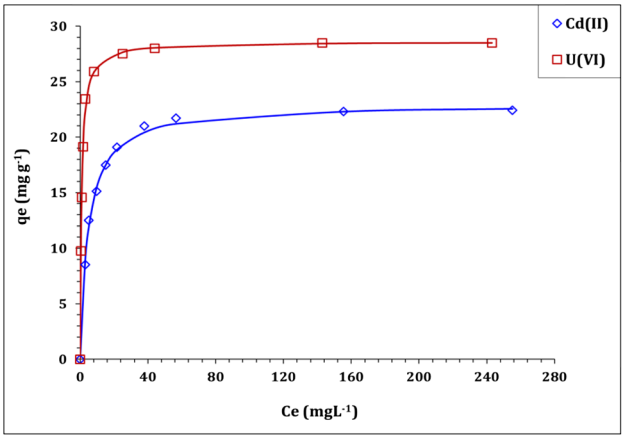

Fig. 8 Isotherm illustrates for metal ions sorption process (temperature 25 ± 1 °C; shaking time 12 h; sorbent dose 4.0 g $L.^{-1}$; pH 4.01)

Table 2 The evaluated variables of Langmuir, Freundlich, and Temkin isotherm models

	Cd(II)	Radioactive species (VI)
Langmuir model		
q_m (mg g^{-1})	23.0	28.6
k_L (L mg^{-1})	0.21	1.16
X^2	0.08	0.05
R^2	0.99	0.99
Freundlich model		
$1/n_F$	0.1	0.1
k_F (mg g^{-1}) (mg L^{-1})	11.0	18.3
X^2	2.72	5.63
R^2	0.77	0.82
Temkin model		
b_T (J mol^{-1})	659.3	896.6
A_T (L g^{-1})	5.7	571.5
X^2	1.83	3.90
R^2	0.81	0.86

the availability of active function groups on the corn carbon surface for binding to metal ions [49, 50]. The second part is characterized by slightly increase in the sorption capacity (plateau) owned to that almost the function groups on the sorbent surface became saturated [49, 50]. The obtained experimental results are analyzed using three isotherm models: Langmuir, Freundlich, and Temkin models. Table 2 declares the variables of the isotherm models.

The displayed data obvious that cadmium and radioactive species (VI) ions sorption process is obeyed to Langmuir model, whereas it exhibits the lowest (x^2) values (0.08 and 0.05) and the highest (R^2) values (0.99) for both cadmium (II) and radioactive (VI) ions respectively. This indicates that the removal is a monolayer process, and corn carbon has a

homogenous surface which is consistent with the TEM analysis (Fig. 6). The isotherm profile of corn carbon towards Cd(II) is consistent with the isotherm profile of magnetic biochar modified with molybdenum disulfide (MoS_2@MBC) [14], titanium-modified ultrasonic biochar [51], and corn straw magnetic biochar composite [15]. Moreover, Aslani and Amik [17], Alahabadi et al. [48], Li et al. [49] reported the same isotherm performance for radioactive ions (VI) uptake using active carbon/PAN composite, wastes-activated carbon, and rice husk magnetic biochar composites respectively is endothermic, spontaneous, and feasible sorption process which is consistent with the obtained data in this work. Freundlich constant ($1/n_F$) is $0.1 < 1/n_F < 0.5$ for carbon and radioactive species ions that indicates that the uptake process is favorable [18]. The calculated sorption capacity qm for cadmium (II) and radioactive ions (VI) (23.0 and 28.6 mg g^{-1}) is close to the experimental sorption capacity (Cd(II): 22.4 mg g^{-1}, and radioactive species (VI): 28.5 mg g^{-1}).

It is worth noted that CS-C possesses higher affinity for radioactive ions (VI) than cadmium (II). There are several parameters affecting the tendency of sorbents towards the metal ions such as hydration energy, metal ion electronegativity, and hydration ion radii [5]. The increase in hydration energy enhances the sorbent affinity; however, the increase in ion electronegativity and hydration ion radii decreases the sorbent affinity towards metal ions radii [52]. The affinity of the applied corn biochar could be elucidated in regards to the variation of hydration energy of both metal ions. The hydration energy of radioactive ions (VI) (− 3958 kJ. mol^{-1}) is higher than that of cadmium(II) (− 1807 kJ. mol^{-1}) [34], which reflects higher sorbent tendency for radioactive (VI) species than cadmium(II). This matches with the obtained data. In regards to the Pearson Hard and Soft Acids and Bases (HSAB) theory, Cd(II) is considered as soft acid while radioactive ions (VI) is classified as hard acid [5]. Ions of radioactive metal (VI) processes higher Lewis acid strength (0.86) than cadmium (0.32) [34]. According to Fig. 2, the main active function groups on the corn bio-char are amine, carbonyl, and hydroxyl groups which are classified as strong bases. This means that the applied carbon will have higher affinity to radioactive (VI) ions (hard acid) than cadmium(II) ions (soft acid), which is consistent with the experimental results. This indicates that the affinity of corn sorbents towards cadmium(II) and radioactive (VI) ions could be explained based on HSBA theory.

The sorption performance of corn carbon for metal ions was displayed in Table 3 in comparison with other sorbents. The explored data declares that sorption capacity of corn carbon is moderate in regards to the displayed sorbents.

3.2.3 Sorption kinetic

The sorption kinetic of heavy metals sorption from multi-component solution using CS-C has been performed. In this regard, a set of experiments were conducted at deferent shaking time of 2–600 min, while other variables were kept at sorbent dose of 4.0 g L^{-1}, solution pH 4.01, 25 ± 1 °C temperature, and initial concentration of 50 mg L^{-1}. The variation of the sorption capacities (qe) VIS time (kinetic curve) was displayed in Fig. 9. The explored results are obvious that the kinetics profile of both

Table 3 The sorption capacity of corn carbon for Cd(II) and radioactive species (VI) in comparison with other carbonaceous materials

Co, mg L^{-1}	Temp, K	pH	Time, h	Qe, mg g^{-1}		Ref
Cadmium (II)						
2–50	298	6.0	24	37.2	MnO2-modified biochar (MBC)	[18]
10–150	298	6.0	6	16.4	Corn straw magnetic biochar at 600 ℃	[14]
10–100	293	6.0	48	41.1	Biochar modified with shrimp bran	[50]
5–1000	298	5.5	24	14.5	Oyster shell biochar	[47]
20–200	298	6.8	24	39.8	Acrylonitrile-modified biochar	[53]
0–20	298	4.5	24	15.5	KOH-modified biochar	[19]
0–120	298	10	24	8.1	Modified rice straw	[54]
20–300	**298**	**4.0**	**12**	**21.3**	**Corn carbon**	**PW**
Radioactive ions (VI)						
20–300	298	5.5	1	27.2	Eucalyptus wood biochar	[55]
5–100	293	4.0	6	19.4	Fungus Pleurotus ostreatus	[56]
10–80	298	10	7	53.2	Modified rice husk biochar	[6]
10–110	298	6.0	1	62.7	Pine needles biochar by HTC	[57]
2–60	318	4.0	24	52.6	Rice husk magnetic biochar composites	[49]
2–100	298	3.0	1.5	92.0	Biochar fibers	[25]
20–300	**298**	**4.0**	**12**	**28.6**	**Corn carbon**	**PW**

The bold is for present work

PW, present work

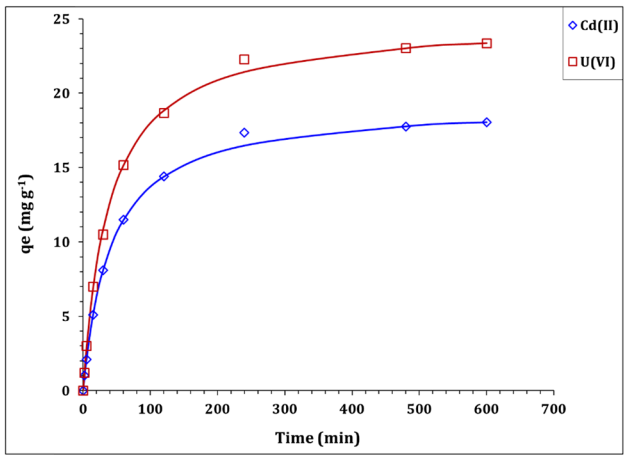

Fig. 9 Kinetic curve for sorption process (4.0 g sorbent/L; initial concentration 50 mg $L.^{-1}$; temperature 25 ± 1 °C; pH 4.01)

Table 4 The evaluated kinetic parameters, pseudo-first-order, pseudo-second-order models

Sorbents	Cd(II)	Radioactive species (VI)
Pseudo-first-order model		
q_1 (mg g^{-1})	17.8	23.0
$k_1 \times 10^3$ (min^{-1})	20.30	20.26
X^2	0.56	0.87
R^2	0.99	0.99
Pseudo-second-order model		
q_2 (mg g^{-1})	19.3	24.9
$k_2 \times 10^3$ (min^{-1})	1.27	1.04
h (mol g^{-1} h^{-1})	0.5	0.6
$t_{1/2}$ (h)	40.9	38.6
X^2	0.06	0.06
R^2	1.00	1.00

metal ions are the same, whereas the sorption capacity rapidly increases with the increment of time increases until the equilibrium state (240 min). This could be attributed to the availability of active function groups on the CS-C surface [35, 36]. The sorption capacity at equilibrium is about 17.3 and 22.3 mg g^{-1} for Cd(II) and radioactive (VI) ions respectively. Prolonging the equilibrium state exhibits a slow rate of reaction and almost a constant sorption capacity. This could be explained based on the surface-active function groups saturation [35, 36]. Lagergren and pseudo-second-order kinetic models were used to explore the sorption kinetics of Cd(II) and radioactive (VI) ions. The nonlinear fit plots for Lagergren and pseudo-second-order kinetic models were displayed in Figs. 2S and 3S respectively. The kinetic parameters as well as the Chi-square and coordination coefficients were displayed in Table 4.

The displayed results are obvious that the pseudo-second-order model possesses the lowest Chi-square coefficient (0.06) and coordination coefficient (1.00) for cadmium(II) and radioactive (VI) ions respectively. In addition, the calculated sorption capacity values (19.3 and 24.9 mg g^{-1}) for Cd(II) and radioactive (VI) respectively are close to the experimental sorption capacity values at equilibrium. This means that the pseudo-second-order kinetic model describes well the uptake of cadmium and radioactive ions using CS-C. This reflects that the uptake is a chemisorption process, and there is an electron sharing between the cadmium and radioactive ions and surface active sites on the CS_C material [48, 49]. Luo et al., and Tao et al., reported that the uptake of cadmium(II) using biochar prepared from corncob and corn straw silage respectively was obeyed to the pseudo-second-order kinetic model [46, 53]. The capture of radioactive (VI) using active carbon/PAN composite [17], wood wastes activated carbon [48], and rice husk magnetic biochar composites [49] has been also obeyed to pseudo-second-order kinetic model.

It is notably that, the values of the half equilibrium time and the initial sorption rate for cadmium(II) (40.9 h; 0.06 mol g^{-1} h^{-1}) are close to the values of radioactive (VI) (38.3 h; 0.06 mol g^{-1} h^{-1}) which confirms the same kinetic performance of both metal ions.

Morris-Weber model could be applied to explore the heavy metals sorption mechanism. In regards to this model, the uptake process is controlled with one solo mechanism (i.e., the intraparticle diffusion (IPD)) in case the Morris-Weber plot exhibits a linear relationship passing through the origin; however, it controlled with a multiple mechanism in case the plot consists of several segments (each segment represents a mechanism) [35, 36]. Figure 10 (Morris-Weber model plot) obviously shows that metal ions sorption process is characterized by multi-linear relationship which indicates that the sorption mechanism is controlled by several mechanisms, i.e., chemical reaction at the beginning of the sorption process until reaching equilibrium then IPD becomes the controlling mechanism [35, 36]. Morris-Weber model variables (Table 5) explore the following: the sorption process has high rate of reaction and low boundary layer effect which means rapid sorption rate of reaction until the equilibrium (first stage). This behavior is attributed to the availability of active sites [15, 16]. While after equilibrium, the sorption process is characterized by low rate of reaction and high boundary layer effect, which indicates slow sorption rate of reaction (second stage). This performance attributed to the fullness of the active function groups on the CS-C surface and the IPD mechanism take place [1–5, 16]. Cadmium(II) and radioactive ions (VI) sorption from aqueous solution using molybdenum disulfide-modified magnetic biochar (MoS2@MBC) [14] and hydroxyapatite-biochar nanocomposite [48] respectively are also characterized with multiple mechanisms sorption reaction.

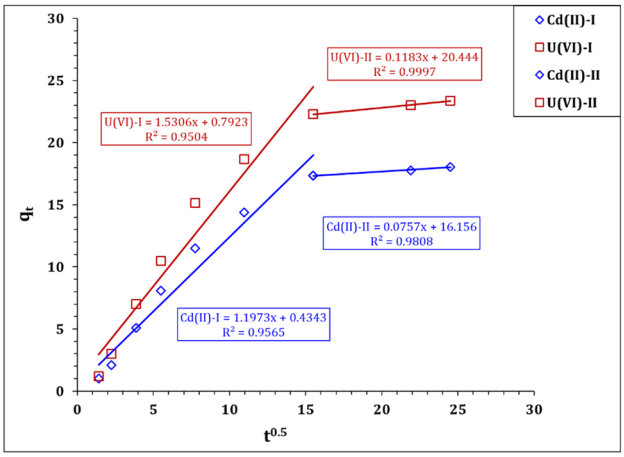

Fig. 10 Morris-Weber model illustrates for sorption process (4.0 g sorbent/L; initial concentration 50 mg $L.^{-1}$; temperature 25 ± 1 °C; pH 4.01)

Table 5 The evaluated parameters of Morris-Weber model kinetic model

		Cd(II)	Radioactive species (VI)
Weber and Morris model	Stage I		
	k_i (mg/g $min^{1/2}$)	1.19	1.53
	C	0.43	0.79
	R^2	0.95	0.95
	Stage II		
	k_i (mg/g $min^{1/2}$)	0.07	0.11
	C	16.1	20.4
	R^2	0.98	0.97

3.2.4 Sorption thermodynamics

The influence of reaction temperature on heavy metals adsorption from aqueous solution using CORN bio-char has been carried out and displayed in Fig. 11. The experimental conditions were shaking time of 12 h, sorbent dose of 4.0 g L^{-1}, solution pH 4.01, and initial concentration range of 50 mg L^{-1}. The displayed data shows that the sorption efficiency is slightly enhanced with the increase in reaction temperature. Van't Hoff plot has been illustrated by the variation of log k_c versus (1/T) and shown in Fig.4S. Table 6 exhibited the values of the thermodynamic parameters (i.e., $\Delta H°$, $\Delta G°$, and $\Delta S°$) The anticipated data declare the endothermic nature of the sorption process whereas $\Delta H°$ has positive values (cadmium(II): 26.8 and radioactive ions (VI): 30.36 kJ mol^{-1}) [32, 33]. Gibbs free energy ($\Delta G°$) of both metal ions exhibits negative values for all reaction temperatures which indicate that the sorption process is spontaneous and feasible reaction. In addition, the decrease of ($\Delta G°$)

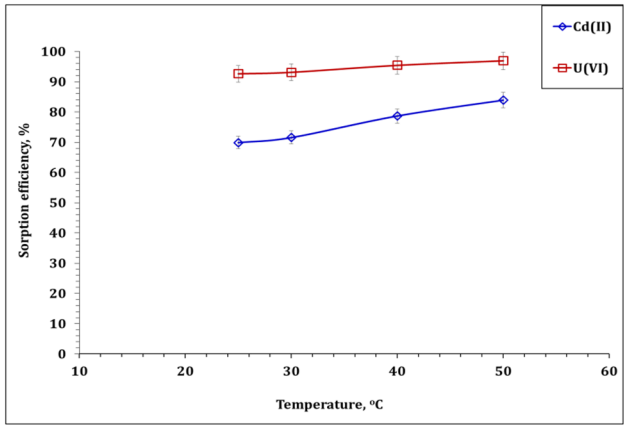

Fig. 11 The removal efficiency of cadmium and radioactive ions against reaction temperature (initial concentration 50 mg $L.^{-1}$; shaking time 12 h; 4.0 g sorbent/L; pH 4.01)

within the temperature increase reveals that the sorption process is more favorable at high temperature [53, 54]. The randomness increment at the solid–liquid interface could be explored from the positive values of ΔS° for uptake process [53, 54]. The same thermodynamic performance (i.e., endothermic, spontaneous, and feasible sorption process) was described for cadmium ions sorption from aqueous solution using corn straw magnetic biochar composite [15], magnetic biochar modified with molybdenum disulfide (MoS2@MBC) [14], and titanium-modified ultrasonic biochar [51]. In addition, Aslani and Amik [17], Alahabadi et al. [48], and Li et al. [49] mentioned the same thermodynamic attitude (endothermic, feasible, and spontaneous) for radioactive ions (VI) uptake using active carbon/PAN composite, wood wastes-activated carbon, and rice husk magnetic biochar composites respectively.

3.2.5 Sorption mechanism

The sorption performance of biochar for metal ions is different and mainly depends on various parameters such as the chemistry of the metal ion in solution and the properties of the biochar such as porous structure, specific surface area, and the surface function groups [14–16]. The adsorption of metal ions using biochar involves several mechanisms including physical adsorption, precipitation, ion exchange, complexation, and electrostatic interaction [58–60]. Several studies mentioned that metal ions sorption using biochar was mainly dominated with the precipitation of metal ions with minerals contained in the biochar [60]. However, Chang et al., and Tan et al., reported that cation exchange mechanism effectively contributes the sorption of metal ions from aqueous solution [59]. The surface complexation between cadmium and radioactive ions with the oxygen-containing functional groups of the biochar is considered to be a crucial sorption mechanism

[4]. Cation-π interactions mechanism is involved for metal ions sorption using biochars with highly cyclic aromatic structure whereas the biochar can be used as π-donor [59, 60]. The electrostatic attraction mechanism is expected for metal ions sorption using biochar with pHpzc < solution pH whereas the biochar surface becomes negatively charged and thus, attracted to the positive cation species [4]. The large surface area and proper micropore structure of biochar enhance the contribution of physical adsorption mechanism for the removal of metal ions from aqueous solution [59–60].

In the present study, the sorption isotherm is obvious that the uptake process is fitting well the Langmuir model (Table 3) which indicates the monolayer sorption through chemical reaction (e.g., ion exchange or surface complexation reaction) between surface function groups and metal ions [14]. The speciation of cadmium(II) and radioactive (VI) ions over solution pH clears that both metal ions are mainly present as divalent cations Cd^{2+} and UO_2^{2+} over solution pH range 1–4 (Fig. 1S-I-II). In addition, zeta potential values of the applied sorbent indicates that the sorbent has negatively charged surface within the pH range indicating that the electrostatic attraction mechanisms effectively contribute on the sorption process; however, the removal of cadmium(II) and radioactive (VI) ions from aqueous solution is predominantly via surface complexation mechanism [60]. Sorption kinetics which is fitted well with pseudo-second-order model (Table 4) indicates that heavy metals sorption using CS-C achieved via the inner sphere surface complex mechanism [46, 59].

This observation is confirmed by FTIR analysis for CS-C sorbent (Fig. 2) which is obvious that the surface of the applied sorbent has plentiful oxygen-containing function groups such as –OH, –COOH, -R-OH, which suggests the complex formation between these (O-) containing function groups and metal ions. This means that the inner sphere surface complexation reaction could be the crucial sorption mechanism [14]. The same sorption mechanism has been reported in previous study for cadmium(II) and radioactive (VI) sorption from aqueous solution using Canna indica-derived biochar [58], rice straw biochars [59], oyster shell waste [60], activated carbon from wood wastes [48], and active carbon/PAN composite [17].

The surface area as well as the porous structure of the applied CS-C suggests that the physical sorption mechanism could contribute in the sorption process [57–60]. Kinetic analysis using Morris-Weber model (Fig. 5) reflects that metal ions uptake from aqueous solution using CS-C is controlled with multiple mechanism, which suggested that at the beginning of the reaction, the inner surface complexation becomes the predominate sorption mechanism (chemical reaction), whereas there are enough surface function groups. However, after equilibrium, the intraparticle diffusion of the metal ions over the sorbent pores becomes the main controlling mechanism (physical reaction) for the sorption process, whereas most of the surface function groups are saturated [60]. The proposed sorption mechanisms could be displayed in Fig. 12.

Table 6 The evaluated thermodynamic parameters

	ΔG (kJ/ mol)				ΔH	ΔS
	25 °C	30 °C	40 °C	50 °C	(kJ/mol)	(J/mol K)
Cadmium (II)	−17.48 ± 0.02	−17.97 ± 0.01	−19.57 ± 0.02	−21.12 ± 0.03	26.83 ± 0.02	148.7 ± 0.2
Radioactive ions (VI)	−21.66 ± 0.03	−22.21 ± 0.02	−24.06 ± 0.02	−25.93 ± 0.04	30.36 ± 0.01	174.5 ± 0.1

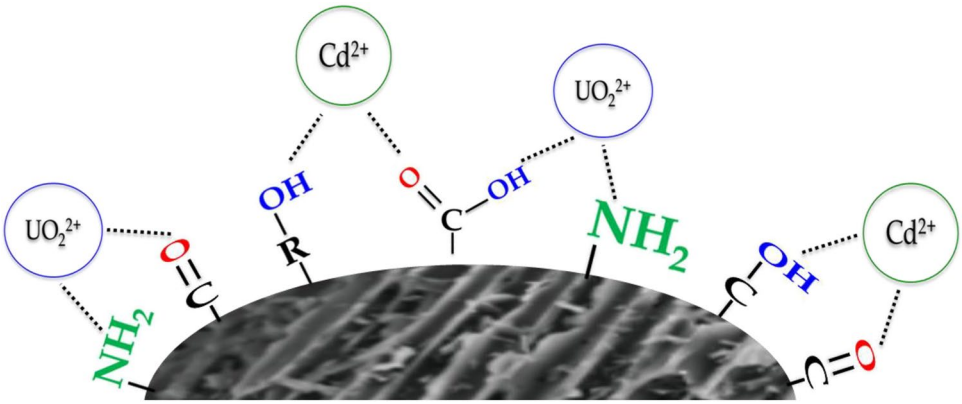

Fig. 12 The proposed sorption mechanisms for sorption process

4 Conclusion

In the present study, corn-shell (solid waste)-based carbon (CS-C) was successfully synthesized. The prepared carbon species were characterized using TEM, BET surface area, Raman, FTIR, XRD, and zeta analyses. After acquiring all the structural, textural, and surface charge characteristics of CS-C, it was forwarded to the process of adsorbing heavy metals from a contaminated aqueous solution through batch technique. The adsorption capacities could be observed at an equilibrium time of 4 h. Isotherm and kinetic modeling of the sorption process clarified that the sorption results obeyed both Langmuir and pseudo-second-order models. The interaction of CS-C sorbent with heavy metal ions was endothermic, spontaneous, and feasible reaction.

Supplementary information The online version contains supplementary material available at https://doi.org/10.1007/s13399-023-04057-4.

Author contribution Ayman F. Abou-Hadid: conceptualization, supervision, and reviewing. Usama A. El-Behairy: conceptualization, supervision and reviewing. Mahmoud M. Elmalih: experimental operation, data interpretation, writing—editing. Enas Amdeha: synthesis, characterization, data curation and interpretation, writing—original draft. Ahmed M. A. El Naggar: methodology, investigation, data curation and interpretation, writing—original draft, reviewing, and editing. Mohamed H. Taha: methodology, validation, data curation, and interpretation, writing—original draft, reviewing, and editing. Ahmed E. M. Hussein: conceptualization, supervision, and reviewing.

Funding Open access funding provided by The Science, Technology & Innovation Funding Authority (STDF) in cooperation with The Egyptian Knowledge Bank (EKB).

Data availability All obtained data during this work are included in this manuscript.

Declarations

Ethical approval The manuscript is prepared in compliance with the publishing ethics policy.

Competing interests The authors declare no competing interests.

Open Access This article is licensed under a Creative Commons Attribution 4.0 International License, which permits use, sharing, adaptation, distribution and reproduction in any medium or format, as long as you give appropriate credit to the original author(s) and the source, provide a link to the Creative Commons licence, and indicate if changes were made. The images or other third party material in this article are included in the article's Creative Commons licence, unless indicated otherwise in a credit line to the material. If material is not included in the article's Creative Commons licence and your intended use is not permitted by statutory regulation or exceeds the permitted use, you will need to obtain permission directly from the copyright holder. To view a copy of this licence, visit http://creativecommons.org/licenses/by/4.0/.

References

1. Da'ana DA, Zouari N, Ashfaq MY, Abu-Dieyeh M, Khraisheh M, Hijji YM and Al-Ghouti MA (2021) Removal of toxic elements and microbial contaminants from groundwater using low-cost treatment options. Current Pollut Rep 7(3):300-324
2. Liang L, Xi F, Weishou Tan Xu, Meng BH, Wang X (2021) Review of organic and inorganic pollutants removal by biochar and biochar-based composites. Biochar 3:255–281
3. Xiao J, Hu R, Chen G, Xing B (2020) Facile synthesis of multifunctional bone biochar composites decorated with Fe/Mn oxide micro-nanoparticles. Physicochemical properties heavy metals sorption behavior and mechanism. J Hazard Mater 399:123067. https://doi.org/10.1016/J.JHAZMAT.2020.123067
4. Xu X, Cao X, Zhao L (2013) Comparison of rice husk- and dairy manure-derived biochars for simultaneously removing heavy metals from aqueous solutions: role of mineral components in biochars. Chemosphere 92(8):955–961. https://doi.org/10.1016/J.CHEMOSPHERE.2013.03.009
5. Hassanein TF, Masoud AM, Mohamed WS, Taha MH, Guibal E (2021) Synthesis of polyamide 6/nano-hydroxyapatite hybrid (PA6/n-HAp) for the sorption of rare earth elements and uranium. J Environ. Chem. Eng 9(1):104731. https://doi.org/10.1016/J.JECE.2020.104731
6. Wang S, Guo W, Gao F, Wang Y, Gao Y (2018) Lead and uranium sorptive removal from aqueous solution using magnetic and nonmagnetic fast pyrolysis rice husk biochars. RSC Adv 8(24):13205–13217. https://doi.org/10.1039/C7RA13540H
7. Khawassek YM, Masoud AM, Taha MH, Hussein AEM (2018) Kinetics and thermodynamics of uranium ion adsorption from waste solution using Amberjet 1200 H as cation exchanger. J Radioanal Nucl Chem 315(3):493–502. https://doi.org/10.1007/S10967-017-5692-1/FIGURES/13
8. Chen YG, Wang Q, Wołowicz A, Gładysz-Płaska A, Wawrzkiewicz M, Sofińska-Chmiel W, Lv GY, Kołodyńska D, Chen SH (2021) Medical plant extract purification from cadmium (II) using modified thermoplastic starch and ion exchangers. Materials 14(16):4734
9. Routzomani A, Lada ZG, Angelidou V, P Raptopoulou C, Psycharis V, Konidaris KF, Chasapis CT and Perlepes SP (2022) Confirming the molecular basis of the solvent extraction of cadmium (II) using 2-pyridyl oximes through a synthetic inorganic chemistry approach and a proposal for more efficient extractants. Molecules 27(5):1619
10. Ali MM, Taha MH, Killa HM, Abd El Wanees S, El-Maadawy MM (2014) Synergistic extraction of uranium from acidic sulfate leach liquor using D2EHPA mixed with TOPO. J Radioanal Nucl Chem 300(3):963–967. https://doi.org/10.1007/S10967-014-3094-1/TABLES/2
11. Mousa MA, Gado HS, Abdelfattah MMG, Madi AE, Taha MH, Roshdy OE (2013) Removal of uranium from crude phosphoric acid by precipitation technique. Arab J. Nucl. Sci. Appl. 5(46):38–47
12. Wang Y, Zheng K, Jiao Z, Zhan W, Ge S, Ning S, Fang S, Ruan X (2022) Simultaneous removal of Cu2+, Cd2+ and Pb2+ by modified wheat straw biochar from aqueous solution: preparation, characterization and adsorption mechanism. Toxics 10(6):316
13. Elzoghby AA, Bakry A, Masoud AM, Mohamed WS, Taha MH, Hassanein TF (2021) Synthesis of polyamide-based nanocomposites using green-synthesized chromium and copper oxides

nanoparticles for the sorption of uranium from aqueous solution. J Environ Chem Eng 9(6):106755
14. Khan ZH, Gao M, Qiu W, Song Z (2020) Properties and adsorption mechanism of magnetic biochar modified with molybdenum disulfide for cadmium in aqueous solution. Chemosphere 255:126995. https://doi.org/10.1016/J.CHEMOSPHERE.2020.126995
15. Khan ZH, Gao M, Qiu W, Islam MS, Song Z (2020) Mechanisms for cadmium adsorption by magnetic biochar composites in an aqueous solution. Chemosphere 246:125701. https://doi.org/10.1016/J.CHEMOSPHERE.2019.125701
16. Younes AA, Masoud AM, and Taha MH (2021) Amino-functionalised cross-linked polyacrylamide for the adsorption of U (VI) ions from contaminated aqueous solutions. *International* Journal of Environmental Analytical Chemistry, 1–14
17. Aslani CK, Amik O (2021) Active carbon/PAN composite adsorbent for uranium removal: modeling adsorption isotherm data, thermodynamic and kinetic studies. Appl. Radiat. Isot 168:109474. https://doi.org/10.1016/J.APRADISO.2020.109474
18. Wu Z, Chen X, Yuan B, Fu ML (2020) A facile foaming-polymerization strategy to prepare 3D MnO2 modified biochar-based porous hydrogels for efficient removal of Cd(II) and Pb(II). Chemosphere 239:124745. https://doi.org/10.1016/J.CHEMOSPHERE.2019.124745
19. Bashir S, Zhu J, Fu Q, Hu H (2018) Comparing the adsorption mechanism of Cd by rice straw pristine and KOH-modified biochar. Environ Sci Pollut Res 25(12):11875–11883. https://doi.org/10.1007/S11356-018-1292-Z/FIGURES/6
20. Dacrory S, Haggag ESA, Masoud AM, Abdo SM, Eliwa AA, Kamel S (2020) Innovative synthesis of modified cellulose derivative as a uranium adsorbent from carbonate solutions of radioactive deposits. Cellulose 27(12):7093–7108. https://doi.org/10.1007/S10570-020-03272-W/FIGURES/8
21. Masoud AM, El-Zahhar AA, El Naggar AM, Zahran AI, Al-Hazmi GA and Taha MH (2022) Soya bean derived activated carbon as an efficient adsorbent for capture of valuable heavy metals from waste aqueous solution. Radiochimica Acta
22. Quyen VT et al (2021) Enhanced recovery of phosphate as a value-added product from wastewater by using lanthanum modified carbon-fiber. Chemosphere 281:130737. https://doi.org/10.1016/J.CHEMOSPHERE.2021.130737
23. Abou-Hadid AF, El-Behairy UA, Elmalih MM, Amdeha E, El Naggar AM, Taha MH, and Hussein AE (2022) Production of efficient carbon fiber from different solid waste residuals for adsorption of hazardous metals from wastewater samples. Biomass Conversion and Biorefinery, pp.1–16
24. Hassan MF, Sabri MA, Fazal H, Hafeez A, Shezad N, Hussain M (2020) Recent trends in activated carbon fibers production from various precursors and applications—a comparative review. J Anal Appl Pyrol 145:104715
25. Liatsou I, Michail G, Demetriou M, Pashalidis I (2017) Uranium binding by biochar fibers derived from Luffa cylindrica after controlled surface oxidation. J Radioanal Nucl Chem 311(1):871–875. https://doi.org/10.1007/S10967-016-5063-3/FIGURES/5
26. Hassan MF, Sabri MA, Fazal H, Hafeez A, Shezad N, Hussain M (2020) "Recent trends in activated carbon fibers production from various precursors and applications a comparative review" J Anal. Appl. Pyrolysis 145:104715. https://doi.org/10.1016/J.JAAP.2019.104715
27. Tan W et al (2021) Removal of levofloxacin through adsorption and peroxymonosulfate activation using carbothermal reduction synthesized nZVI/carbon fiber. Chemosphere 280:130626. https://doi.org/10.1016/J.CHEMOSPHERE.2021.130626
28. Surya K, Michael MS (2020) Novel interconnected hierarchical porous carbon electrodes derived from bio-waste of corn husk for supercapacitor applications. J Electroanal. Chem 878:114674. https://doi.org/10.1016/J.JELECHEM.2020.114674
29. Binh QA, Nguyen VH, Kajitvichyanukul P (2022) Influence of pyrolysis conditions of modified corn cob bio-waste sorbents on adsorption mechanism of atrazine in contaminated water. Environ Technol Innov 26:102381
30. Chailuecha C, Klinbumrung A, Chaopanich P, Sirirak R (2021) Graphene-like porous carbon nanostructure from corn husk: synthesis and characterization. Mater Today Proc 47:3525–3528. https://doi.org/10.1016/J.MATPR.2021.03.512
31. Jarernboon W, Iamtipueng P, Pimanpang S, Amornkitbamrung V (2018) Preparation of the natural carbon fiber from narrow-leaved cattails (Typha angustifolia Linn.) flower for using as the cathode catalyst in the zinc-air fuel cell. Mater Today Proc 5(6):14002–14008. https://doi.org/10.1016/J.MATPR.2018.02.052
32. AM Masoud (2020) "Sorption behavior of uranium from sulfate media using purolite A400 as a strong base anion exchange resin," https://doi.org/10.1080/03067319.2020.1763974.
33. B. S. Marques TS, Frantz TR, Sant'Anna Cadaval Junior LA de Almeida Pinto, and GL Dotto (2019) "Adsorption of a textile dye onto piaçava fibers: kinetic, equilibrium, thermodynamics, and application in simulated effluents," Environ. Sci. Pollut. Res. Int., 26(28) 28584–28592 https://doi.org/10.1007/S11356-018-3587-5
34. Taha MH (2021) Sorption of U(VI), Mn (II), Cu(II), Zn(II), and Cd(II) from multi-component phosphoric acid solutions using MARATHON C resin. Environ Sci Pollut Res Int 28(10):12475–12489. https://doi.org/10.1007/S11356-020-11256-3
35. Kang HJ, Kim JH (2019) Adsorption kinetics, mechanism, isotherm, and thermodynamic analysis of paclitaxel from extracts of taxus chinensis cell cultures onto sylopute. Biotechnol Bioprocess Eng 24(3):513–521. https://doi.org/10.1007/S12257-019-0001-1
36. MH Taha (2020) "Solid-liquid extraction of uranium from industrial phosphoric acid using macroporous cation exchange resins: MTC1600H, MTS9500, and MTS9570," https://doi.org/10.1080/01496395.2020.1787446 1–17, 2020, https://doi.org/10.1080/01496395.2020.1787446
37. Chaudhuri B, Ghosh S, Mondal B, Bhadra D (2022) "Preparation and characterization of carbon fibre powder (CFP)-polyvinyl alcohol (PVA) composite films showing percolation threshold behaviour" Mater. Sci. Eng. B 275:115500. https://doi.org/10.1016/J.MSEB.2021.115500
38. Poursorkhabi V, Abdelwahab MA, Misra M, Khalil H, Gharabaghi B, Mohanty AK (2020) Processing, carbonization, and characterization of lignin based electrospun carbon fibers: a review. Front Energy Res 8:208. https://doi.org/10.3389/FENRG.2020.00208/BIBTEX
39. Shi L, Sessim M, Tonks MR, Phillpot SR (2021) Generation and characterization of an improved carbon fiber model by molecular dynamics. Carbon N Y 173:232–244. https://doi.org/10.1016/J.CARBON.2020.11.011
40. Taha MH, Abdel Maksoud SA, Ali MM, El Naggar AMA, Morshedy AS, Elzoghby AA (2019) Conversion of biomass residual to acid-modified bio-chars for efficient adsorption of organic pollutants from industrial phosphoric acid: an experimental, kinetic and thermodynamic study. 9912 211–1234. https://doi.org/10.1080/03067319.2019.1618459
41. Morshedy AS, Taha MH, El-Aty DMA, Bakry A, El Naggar AMA (2021) Solid waste sub-driven acidic mesoporous activated carbon structures for efficient uranium capture through the treatment of industrial phosphoric acid. Environ. Technol. Innov. 21:101363. https://doi.org/10.1016/J.ETI.2021.101363
42. Qu W, Liu J, Xue Y, Wang X, Bai X (2018) Potential of producing carbon fiber from biorefinery corn stover lignin with high ash content. J Appl Polym Sci 135(4):45736. https://doi.org/10.1002/APP.45736
43. Raimundo RA et al (2022) Synthesis and characterization of NiFe-carbon fibers by solution blow spinning and application for the

oxygen evolution reaction. J. Phys. Chem. Solids 160:110311. https://doi.org/10.1016/J.JPCS.2021.110311
44. Liu F, Wang H, Xue L, Fan L, Zhu Z (2008) Effect of microstructure on the mechanical properties of PAN-based carbon fibers during high-temperature graphitization. J Mater Sci 43(12):4316–4322. https://doi.org/10.1007/S10853-008-2633-Y
45. Lai C et al (2014) Free-standing and mechanically flexible mats consisting of electrospun carbon nanofibers made from a natural product of alkali lignin as binder-free electrodes for high-performance supercapacitors. J Power Sources 247:134–141. https://doi.org/10.1016/J.JPOWSOUR.2013.08.082
46. Tao Q et al (2019) Enhanced Cd removal from aqueous solution by biologically modified biochar derived from digestion residue of corn straw silage. Sci Total Environ 674:213–222. https://doi.org/10.1016/J.SCITOTENV.2019.03.438
47. Lian W et al (2021) Influence of pyrolysis temperature on the cadmium and lead removal behavior of biochar derived from oyster shell waste. Bioresour. Technol. Reports 15:100709. https://doi.org/10.1016/J.BITEB.2021.100709
48. Alahabadi A et al (2020) Activated carbon from wood wastes for the removal of uranium and thorium ions through modification with mineral acid. Colloids Surfaces A Physicochem. Eng. Asp. 607:125516. https://doi.org/10.1016/J.COLSURFA.2020.125516
49. Li M, Liu H, Chen T, Dong C, Sun Y (2019) Synthesis of magnetic biochar composites for enhanced uranium(VI) adsorption. Sci Total Environ 651:1020–1028. https://doi.org/10.1016/J.SCITOTENV.2018.09.259
50. Yin W, Zhao C, Xu J (2019) Enhanced adsorption of Cd (II) from aqueous solution by a shrimp bran modified Typha orientalis biochar. Environ Sci Pollut Res Int 26(36):37092–37100. https://doi.org/10.1007/S11356-019-06658-X
51. Luo M, Lin H, He Y, Li B, Dong Y, Wang L (2019) Efficient simultaneous removal of cadmium and arsenic in aqueous solution by titanium-modified ultrasonic biochar. Bioresour Technol 284:333–339. https://doi.org/10.1016/J.BIORTECH.2019.03.108
52. Lazarević S, Janković-Častvan I, Jovanović D, Milonjić S, Janaćković D, Petrović R (2007) Adsorption of Pb2+, Cd2+ and Sr2+ ions onto natural and acid-activated sepiolites. Appl Clay Sci 37(1–2):47–57. https://doi.org/10.1016/J.CLAY.2006.11.008
53. Luo M, Lin H, Li B, Dong Y, He Y, Wang L (2018) A novel modification of lignin on corncob-based biochar to enhance removal of cadmium from water. Bioresour Technol 259:312–318. https://doi.org/10.1016/J.BIORTECH.2018.03.075
54. Wang S et al (2019) Characterization and interpretation of Cd (II) adsorption by different modified rice straws under contrasting conditions. Sci. Reports 2019 91 9(1):1–13. https://doi.org/10.1038/s41598-019-54337-1
55. Mishra V, Sureshkumar MK, Gupta N, Kaushik CP (2017) Study on sorption characteristics of uranium onto biochar derived from eucalyptus wood. Water. Air. Soil Pollut. 228:8. https://doi.org/10.1007/S11270-017-3480-8
56. Zhao C et al (2016) Characteristics of uranium biosorption from aqueous solutions on fungus Pleurotus ostreatus. Environ Sci Pollut Res Int 23(24):24846–24856. https://doi.org/10.1007/S11356-016-7722-X
57. Bin Zhang Z, Cao XH, Liang P, Liu YH (2013) Adsorption of uranium from aqueous solution using biochar produced by hydrothermal carbonization. J. Radioanal. Nucl. Chem. 295(2):1201–1208. https://doi.org/10.1007/S10967-012-2017-2/FIGURES/12
58. Cui X et al (2016) Potential mechanisms of cadmium removal from aqueous solution by Canna indica derived biochar. Sci Total Environ 562:517–525. https://doi.org/10.1016/J.SCITOTENV.2016.03.248
59. Y Deng, S Huang, C Dong, Z Meng, and X Wang (2020) "Competitive adsorption behaviour and mechanisms of cadmium, nickel and ammonium from aqueous solution by fresh and ageing rice straw biochars," Bioresour. Technol., 303 https://doi.org/10.1016/J.BIORTECH.2020.122853
60. Iber BT, Okomoda VT, Rozaimah SA, Kasan NA (2021) Eco-friendly approaches to aquaculture wastewater treatment: assessment of natural coagulants vis-a-vis chitosan. Bioresour. Technol. Reports 15:100702. https://doi.org/10.1016/J.BITEB.2021.100702

Publisher's note Springer Nature remains neutral with regard to jurisdictional claims in published maps and institutional affiliations.